Catalysis Science & Technology

Accepted Manuscript

This article can be cited before page numbers have been issued, to do this please use: Z. Vajglova, N. Kumar, M. Peurla, J. Peltonen, I. Heinmaa and D. Murzin, *Catal. Sci. Technol.*, 2018, DOI: 10.1039/C8CY01951G.

ROYAL SOCIETY OF CHEMISTRY

rsc.li/catalysis

View Article Online
DOI: 10.1039/C8CY01951G

Synthesis and physico-chemical characterization of Beta-Bentonite composite materials for shaped catalysts

Zuzana Vajglová[1,2], Narendra Kumar[1], Markus Peurla[3], Janne Peltonen[3], Ivo Heinmaa[4], Dmitry Yu. Murzin[1*]

[1] *Åbo Akademi University, Johan Gadolin Process Chemistry Centre, Laboratory of Industrial Chemistry and Reaction Engineering, Biskopsgatan 8, Turku/Åbo, Finland*

[2] *Institute of Chemical Process Fundamentals of the ASCR, v. v. i., Eduard Hála Laboratory of Separation Processes, Rozvojova 2/135 Prague 6, Czech Republic*

[3] *University of Turku, Turku, Finland*

[4] *National Institute of Chemical Physics and Biophysics, Akadeemia tee 23, 12618 Tallinn, Estonia*

**dmurzin@abo.fi, corresponding author*

Abstract

Composite materials for shaped catalysts were prepared from three commercial Beta zeolites using bentonite as an aluminosilicate clay binder. All pristine materials and the synthesized powder mixtures were characterized using X-ray powder diffraction for phase purity and structure, scanning electron microscopy for morphology, transmission electron microscopy for porosity and periodicity, nitrogen physisorption for surface area, pore volume and pore size distribution, Fourier transform infrared spectroscopy using pyridine as a probe molecule to elucidate presence, strength and amount of Brønsted and Lewis acid sites. Elemental analysis was carried out using energy dispersive X-ray micro-analysis.

Through a systematic comparison of the properties of the individual components and powder zeolite−binder composites, the study elucidated the crucial binder influence on the key properties of the catalytic supports already during synthesis of the composites in the powder form, i.e. prior to shaping. It can be concluded that the promoting effect of the bentonite binder is derived from chemical interactions with the zeolite. The resulting effect of the binder on composite properties is not a simple additive just reflecting the nominal ratio of components. The synthesis process, zeolite type (SiO_2/Al_2O_3 ratio of the framework, particle size) and binder concentration play a significant role in the resulting binder effect in composites.

Keywords: composite materials, shaped catalysts, zeolite, clay binder

View Article Online
DOI: 10.1039/C8CY01951G

1 Introduction

Zeolite catalysts bodies are employed on a global scale in important chemical processes, such as synthesis of many bulk chemicals as well as in crude-oil refining [1,2]. There are many papers devoted to explaining the catalytic properties and industrial applications of zeolites [3]. Zeolites are crystalline, micro porous, hydrated aluminosilicates that are built from an infinitely extending three dimensional network of $[SiO_4]^{4-}$ and $[AlO_4]^{5-}$ tetrahedra linked to each other by sharing of oxygen atoms, normally in the 1 – 10 μm particle size range [4-6].

However, if a zeolite based catalyst is to be used at an industrial level, it is shaped into bodies such as granules, spheres, and extrudates. Zeolites are pelletized with a binder to obtain larger and more resistant particles and to avoid an extremely high pressure drop in fixed-bed reactors. Shaping of the zeolite powder into pellets is commercially done using natural clays such as bentonite, attapulgite, and kaolin amounting of 15 – 20% of the zeolite pellet. The overall aim is to obtain the required mechanical strength to resist attrition losses, maintain chemical stability for prolonged use and limit expenditure (among many others), whilst achieving high catalytic activity and selectivity [1, 3, 4, 7, 8].

Although binders might not be catalytically active, binder-zeolite interactions can exert effects on catalytic performance through both physical and chemical means. This makes a marked influence on activity, selectivity, and stability of a zeolite. The binder presence can affect the acidic properties of a zeolite as a result of changes in the ion exchange between zeolite protons and sodium in clay. Other influence can include porosity modifications, trapping coke precursors by the binder, and/or blocking of zeolite channels during pelletization [1, 3, 4, 7-10]. The work of Hargreaves and Munnoch [9] highlights the importance of binder effects that occur in such zeolite based materials. The binder can also influence the catalytic performance of a zeolite by trapping metal poisons such as nickel and vanadium from feedstock of a petrochemical origin [7].

View Article Online
DOI: 10.1039/C8CY01951G

Even if the catalytic properties of the zeolite can be strongly altered, consideration of the binder impact is seldom done in the academic literature. Such considerations are, however, rather important, as some effects can be very prominent for e.g. catalyst promotion and extension of the catalyst lifetime. Due consideration needs to be given not only to the nature of the agents used for binding but also to the method, and the stage of their addition to the catalyst formulations to achieve the optimal technical performance [1-3, 7, 9, 11, 12].

In the recent years, there were significant advancements in the characterization of shaped bodies achieved by Pérez-Ramírez and co-workers [12, 16, 17] as well as by Weckhuysen and co-authors [13-15] using novel characterization methods. These characterization tools allowed probing the multi-dimensional parameters of zeolite-binder materials with a high spatiotemporal resolution and have provided significant insights into the structure–performance relationships of these industrially relevant technical catalysts.

Clay binder minerals are crystalline substances evolved primarily from chemical weathering of certain rock/forming minerals. Chemically, they are hydrous aluminosilicates having metallic ions [18]. Bentonite is a laminar and expandable clay with wet binding properties being widely available throughout the world[7]. The dispersability of clays in aqueous suspensions is the reason for their agglomeration properties. Zeolite particles are surrounded by clay laminae, and when water is removed, a solid phase is obtained in which the zeolite particles are bound by the clay [7]. It has been shown [19] that the acidic forms of clays do not have binding properties while their sodium forms exhibit better performance. Clay minerals are distinguished from other colloidal materials by a highly anisometric and often irregular particle shape, a broad particle size distribution, flexibility of the layers, different types of charges and heterogeneity of the layer charges, a pronounced cation exchange capacity, disarticulation (in case of smectites) and different modes of aggregation [7, 18, 20-24].

View Article Online
DOI: 10.1039/C8CY01951G

In this work, the composite materials for shaped catalysts were prepared from three Beta zeolites (with different SiO_2/Al_2O_3) ratios using the bentonite clay as a binder in different quantities ranging from 10 to 65 wt.%. The study is focused on the influence of SiO_2/Al_2O_3 ratio, clay binder concentration and calcination temperature on key properties of the prepared powder compositions. For clarification, all materials were characterized in detail using several analytical methods.

2 Experimental

2.1 Preparation of the powder mixture of zeolites and binder

Three different commercial Beta zeolites with varying SiO_2/Al_2O_3 ratio were obtained from Zeolyst International, namely NH_4-Beta-25 (CP814E), H-Beta-150 (CP811E) and H-Beta-300 (CP811C-300). The last number in the zeolite reflects the nominal SiO_2/Al_2O_3 molar ratio. The NH_4^+ form of zeolite NH_4-Beta-25 was transformed to the corresponding proton form in a muffle oven using a step calcination procedure: initial temperature 250 °C (held for 50 min), increased at 4 °C/min to 400 °C and held at the final temperature for 4 h. Such treatment is sufficient for a complete conversion of ammonium ions to Brønsted acid sites.

As a binder, aluminosilicate clay bentonite from VWR International was selected. All materials were crushed and sieved into a fraction < 63 µm in a vibratory micro mill (Fritsch).

The zeolite / clay binder mixtures were prepared using a five-step synthesis procedure (Figure 1). This procedure involved dry mixing, wet mixing, evaporation, drying and calcination. In the first step, the H-Beta forms of the catalysts (< 63 µm) and the bentonite binder (< 63 µm) were ground and mixed in a ball mill (Fritsch) for 4 hours. The aim of the ball milling was intensive mixing of the materials and removal of the influence of broad particle size distributions, which indirectly may influence the physico-chemical and catalytic properties. The amount of the bentonite binder was varied in the mixture as follows: 90% H-

View Article Online
DOI: 10.1039/C8CY01951G

Beta + 10% bentonite, 80% H-Beta + 20% bentonite, 70% H-Beta + 30% bentonite and 35% H-Beta + 65% bentonite. The total amount of the mechanical mixture was 5 g. In the second step, 100 mL of distilled water was added to the obtained mixture. The aqueous solution was stirred with 50 rpm at ambient temperature for 24 h. In the subsequent steps, water was evaporated at 40 °C under vacuum and drying was carried out at 100 °C for 7 h. In the final step, the dry mixture was calcined in a step calcination procedure: initial temperature 250 °C (held for 50 min), increased at 4 °C/min to 500 °C and held at the final temperature for 4 h. The resulting mixtures were characterized in detail.

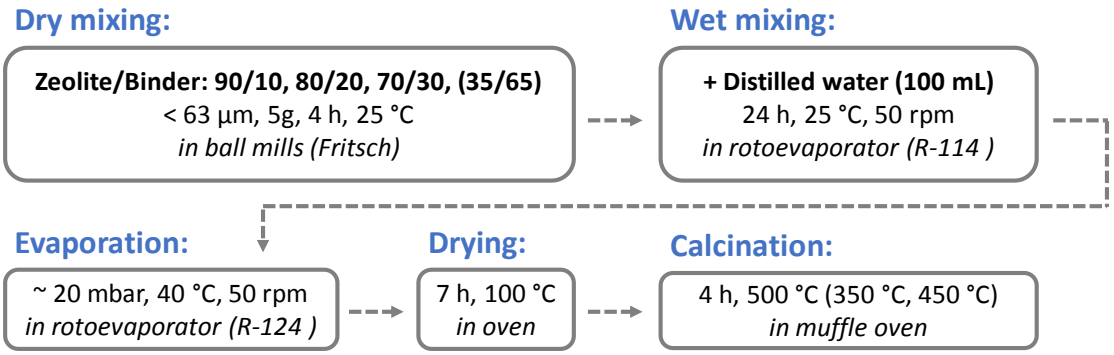

Figure 1.The scheme of a five-step synthesis procedure.

2.2 Characterization of synthesized powder mixtures

2.2.1 X-ray powder diffraction (XRD)

The crystal structure was determined by X-ray diffraction (XRD) with a Philips X'Pert Pro MPD X-ray powder diffractometer. The device was operated in Bragg-Brentano diffraction mode, and the monochromatized Cu-Kα radiation (λ=1.541874 Å) was generated with a voltage of 40 kV and a current of 45 mA. The measured 2θ angle range was 5.0° − 85.0°, with a step size of 0.026° and the measurement time of 100 s per step. The measured diffractograms were analyzed with Philips X'Pert HighScore and MAUD programs.

View Article Online
DOI: 10.1039/C8CY01951G

HighScore together with MAUD was used for the phase analysis and MAUD for the Rietveld refinement.

2.2.2 Scanning electron microscopy (SEM) and energy dispersive X-ray microanalysis (EDX)

Morphological studies were performed by scanning electron microscopy. A scanning electron microscope (Zeiss Leo Gemini 1530) was used for determination of the crystal morphology. Elemental analysis of microporous materials was done by energy-dispersive X-ray microanalysis (Zeiss Leo Gemini 1530). SEM images were obtained by sputtering the samples with a thin carbon coating and using an accelerating voltage of 2.7 kV with ca. 5 – 6 mm working distance.

2.2.3 Transmission electron microscopy (TEM)

Particle size and porosity of materials were characterized by transmission electron microscopy (JEOL JEM-1400Plus) using imaging and electron diffraction functions. The samples were prepared by blowing a powder on the TEM grid with a pipette.

2.2.4 Nitrogen physisorption

Nitrogen-physisorption using Sorptometer 1900 (Carlo Erba Instruments) determined the textural properties of microporous materials. A sample was outgassed at 150 °C for 3 h before each measurement. The Dubinin equation and the Horvath-Kawazoe method[25] were used for calculation of the specific surface area and pore volume, respectively. The measurement temperature was –196 °C.

2.2.5 Fourier transform infrared spectroscopy (FTIR)

The amount of Brønsted and Lewis acid sites was quantified by Fourier transform infrared spectroscopy using pyridine (≥ 99.5%) as the probe molecule (ATI Mattson FTIR Infinity Series). The samples were pressed into thin pellets (10 – 20 mg) and placed in the

View Article Online
DOI: 10.1039/C8CY01951G

measurement cell. Prior to pyridine adsorption, the samples were outgassed under vacuum (0.08 mbar) at 450 °C for 2 h and the background spectra were recorded at 100 °C. Pyridine was adsorbed at 100 °C for 30 min and the spectra were recorded at 100 °C after heating the sample to 250, 350 and 450 °C respectively. The Lewis acidity was quantified from the adsorption band at 1450 cm^{-1} and the Brønsted acidity from the adsorption band at 1550 cm^{-1} using previously reported data of Emeis [26] (integrated molar extinction coefficients = 1.67 and 2.22 cm/μmol for the Brønsted and Lewis acid sites, respectively). The strength of the acid sites is classified based on temperature at which pyridine desorbs from the catalyst, i.e. desorption between 250 – 350°C was ascribed to weak acid sites, while desorption at 350 – 450 °C reflects medium acid sites. Strong acid sites retain pyridine at 450 °C. The catalyst weight in g (m_{cat}) was taken into account in the calculations of weak, medium and strong acid sites (eqns. 1 and 2):

$$\text{C (pyridine on Brønsted acid sites)} = \frac{k_1 \times S \times R^2}{m_{cat}} \quad (1)$$

$$\text{C (pyridine on Lewis acid sites)} = \frac{k_2 \times S \times R^2}{m_{cat}} \quad (2)$$

where C is the number of acid sites per gram of catalyst (μmol/g), k_1 = 1.88, k_2 = 1.42 are coefficients [26] in μmol/cm, R is the radius of the catalyst pellet in cm and S is the average peak area in cm^{-1} from the six integrated absorbances of Brønsted or Lewis bands at a given temperature. For calculation of the strong acid sites S = $S_{450°C}$ (peak area measured at 450 °C) while for medium and weak acid sites the following equations were respectively used S = $S_{350°C} - S_{450°C}$ and S = $S_{250°C} - S_{350°C}$.

View Article Online
DOI: 10.1039/C8CY01951G

2.2.6 ^{29}Si and ^{27}Al MAS NMR analysis

^{29}Si MAS (magic angle spinning) NMR spectra were recorded on Bruker AVANCE-II spectrometer at 14.1 T magnetic field using home-built MAS probe for 4 mm od Si3N4 rotors. Single pulse spectra of 4000 averages were accumulated with 4 μs pulse (0.4 π) excitation at 119.23 MHz with a repetition time of 20 s at 10 kHz sample spinning speed. The chemical shifts are given in tetramethylsilane (TMS) scale.

^{27}Al MAS-NMR spectra were recorded at 208.49 MHz on Bruker AVANCE-III spectrometer for 18.8 T external field using Bruker MAS probe and 3.2 mm zirconia rotors. The spectra were collected by 40000 accumulations with single 0.6 μs pulse (π/18) excitation, repetition time 60 ms and 22 kHz sample spinning frequency. The spectra are referenced to the frequency of $AlNO_3$ solution.

The intensity in the NMR spectra was normalized to the number of accumulations and to the mass of the sample.

3 Results and Discussion

Pristine materials were characterized to explore the influence of SiO_2/Al_2O_3 ratio on their properties. Characterization results of the pristine materials were used as references values for comparison with the characterization data of composites. For this reason and to avoid potential uncertainties because of ball milling, prior to characterization all pristine zeolite materials and pristine bentonite were also sieved into the same fraction (below 63 μm) and underwent the same first and fifth steps of synthesis procedure as mixtures containing bentonite, i. e. steps including ball mixing and calcination.

Characterization of the synthesized powder mixtures was done for different clay binder concentrations and calcination temperatures.

View Article Online
DOI: 10.1039/C8CY01951G

3.1 Effect of clay binder concentration

3.1.1 Elemental analysis

Elemental analysis of pristine materials (Table S1) revealed a clear difference between the SiO_2/Al_2O_3 ratio indicated by the manufacturer (i.e. the last number in the zeolite name) and the measurements. Being valid for H-Beta-25, in the case of H-Beta-150 and H-Beta-300 the measured values of SiO_2/Al_2O_3 molar ratio are significantly lower than the nominal ones. The presence of other substances was not found in pristine Beta zeolites. This excludes introduction of impurity elements from the grinding tools (agate, sintered corundum, zirconium oxide, stainless steel, hardened steel, hard metal tungsten carbide). SiO_2/Al_2O_3 molar ratio of 9 was determined for bentonite. In the pristine bentonite, MgO, K_2O and Fe_2O_3 were observed in small amounts, 1.9 wt.%, 1.5 wt.% and 3.1 wt.%, respectively.

Elemental analysis of the synthesized powder mixtures showed a non-linear dependence of the mixture composition on the bentonite amount (Figure 2). MgO presented in bentonite was observed in the mixtures containing 20 wt.% or more bentonite. At the same time, K_2O was seen in mixtures with up to 30 wt.% bentonite. These results are in line with the expectations, as pristine bentonite contained more MgO (1.9 wt.%) than K_2O (1.5 wt.%). On the contrary, while Fe_2O_3 (3.1 wt.%) is present in the pristine bentonite, it was observed only in the mixture with the largest content of bentonite (i.e. 35 wt.% H-Beta-25 + 65 wt.% bentonite) in 2.3 wt.%. In other composite materials, no Fe content was detected.

A non-linear dependence of the mixture composition on the bentonite amount can be interpreted as a result of ion exchange and interfacial interactions between Beta zeolites and the bentonite binder. An alternative explanation of the non-linear dependence can be related to inhomogeneous mixing of Beta zeolites and the bentonite binder. This in combination of a lower accuracy of the utilized method because of a small area used for detection and a low

View Article Online
DOI: 10.1039/C8CY01951G

concentration of impurities originating from bentonite (MgO, K_2O, Fe_2O_3) can give a non-linear dependence.

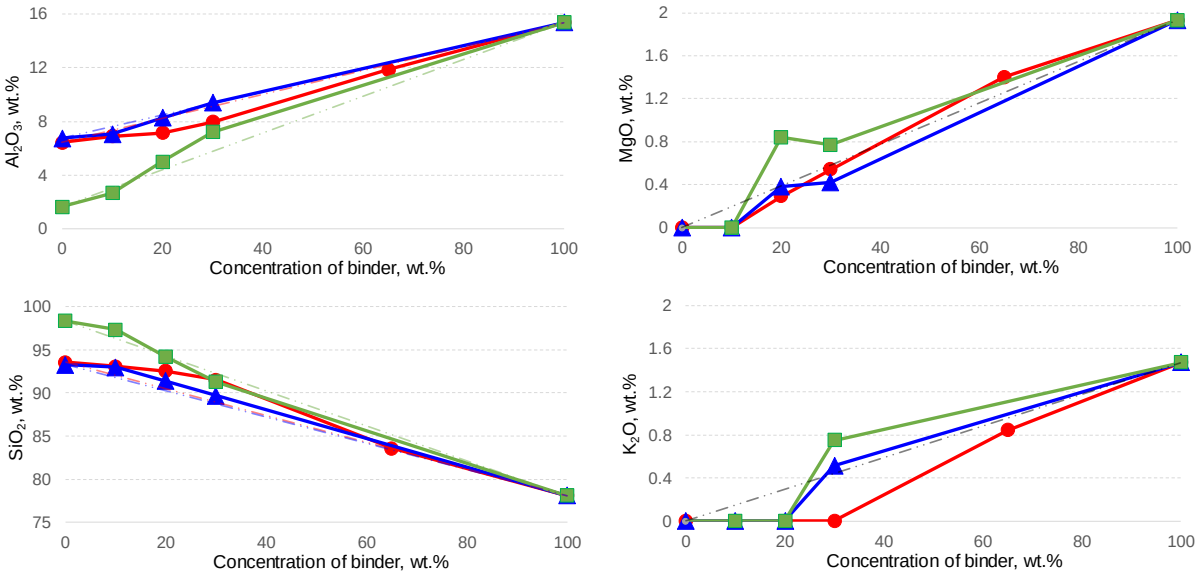

Figure 2. The influence of bentonite concentration on elemental analysis of three types of Beta zeolite. Legend: H-Beta-25 (red circle), H-Beta-150 (blue triangle), H-Beta-300 (green square), nominal-linear dependence (dot-dot-dash line) is shown for illustration purposes.

3.1.2 The phase purity and crystal structure

The phase purity and crystal structure were determined by X-ray diffraction. In Figure S1 XRD patterns of the pristine materials are displayed. In all pristine Beta zeolite materials, the diffraction peaks related to only Beta zeolite polymorph A (100 wt.%, SiO_2 framework) were observed. The crystal size of 7 ± 2 nm was determined by the Rietveld refinement method. The diffractogram of bentonite consisted of peaks originating from illite (80 ± 10 wt.%, monoclinic), montmorillonite (< 5 wt.%, hexagonal), kaolinite (< 5 wt.%, triclinic) and SiO_2 (20 ± 10 wt.%, hexagonal).

For illustration purposes, Figure 3 shows the base units of clay minerals and the main clay minerals observed in the pristine bentonite. Structure of the main clay minerals of bentonite is

based on combined crystal sheets, the tetrahedral (or silica), and the octahedral (or alumina), sheets.

View Article Online
DOI: 10.1039/C8CY01951G

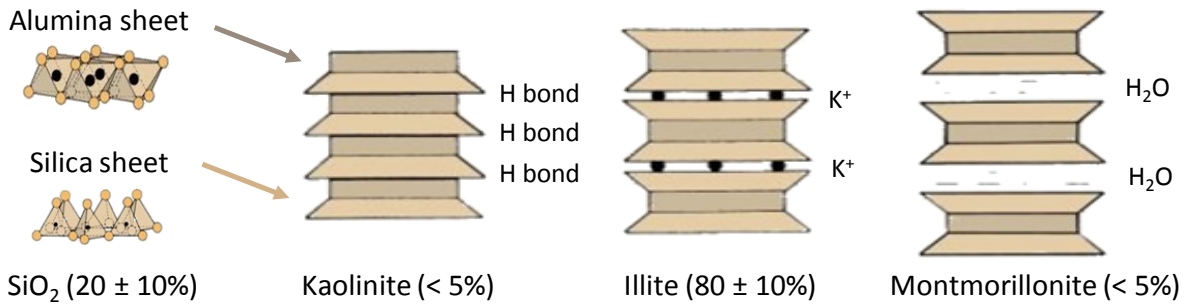

Figure 3. The crystal structure of bentonite [18, 24].

Figure 4 show the X-ray powder diffraction patterns of the pristine H-Beta-25, H-Beta-150, H-Beta-300 zeolites and their counter parts with varying concentrations of bentonite from 10 to 30 wt.%. It can be inferred that modification of H-Beta-25, H-Beta-150, H-Beta-300 with various amounts of bentonite in the crystal form as a binder did not destroyed the parent structure of Beta zeolite. In all synthesized powder mixtures, the intensities of bentonite related peaks (mainly from the illite phase, $2\theta = 19° – 28°$) increased as the amount of bentonite in the sample was increased.

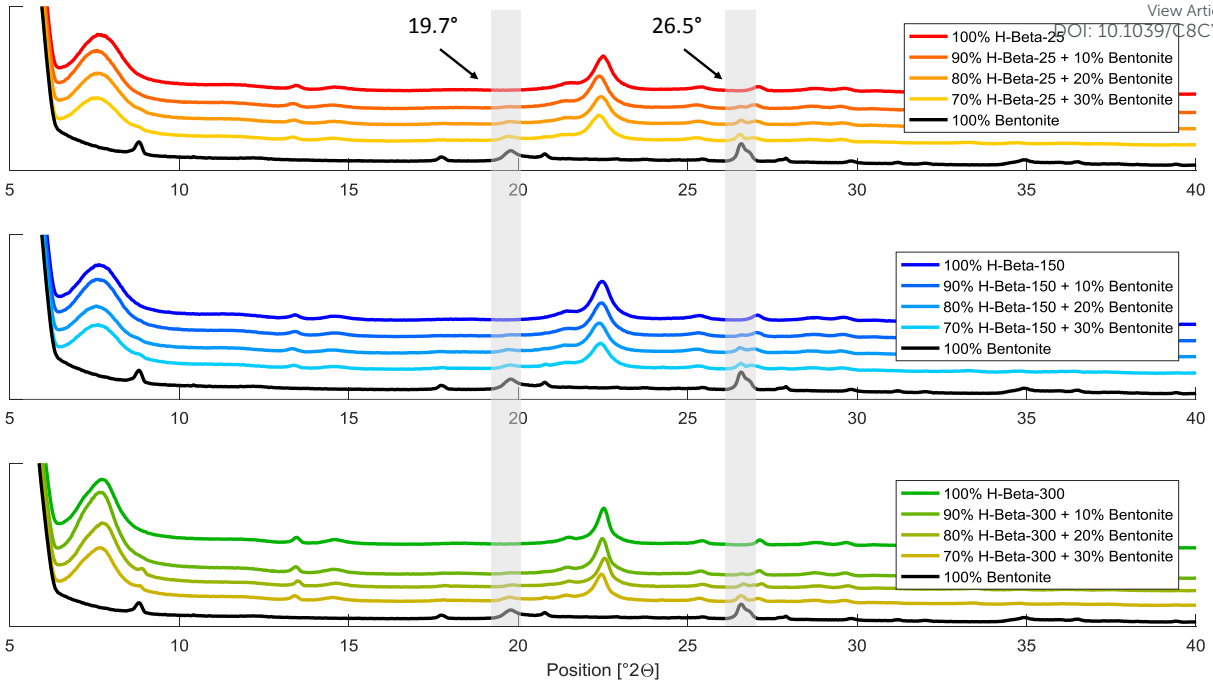

Figure 4. XRD patterns: Effect of the binder concentration.

3.1.3 Morphology, porosity and periodicity

SEM images show that the structure of Beta zeolites does not exclusively contain single crystallites of spherical shape. Beta zeolites contains mainly aggregates of crystals, being also partially amorphous (Figure 5). Note that this a zeolitic catalyst used on the industrial scale in oil refinery processes. H-Beta-25 and H-Beta-150 morphology is almost identical, which is in line with the results of XRD and EDX analysis. The particle size of these materials is 60 nm on average, while the particle size of H-Beta-300 is five times larger (300 nm on average). The structure of bentonite is non-amorphous, mainly consisting of fibers and of platelets with sharp edges (Figure S2). The observed particle size of bentonite being on average just 450 nm could be as large as ca. 28 µm. Based on the work of Das [27] the observed average particle size can be attributed to Illite, while the unique large particles can be attributed to kaolinite. This is in line with the XRD results showed above illustrating that the used bentonite consists of 80% illite and less than 5% kaolinite.

View Article Online
DOI: 10.1039/C8CY01951G

TEM images with a scale bar 1 μm clearly show large differences of the particle size of H-Beta-25 and H-Beta-150 vs. H-Beta-300 and morphology differences of pristine materials (Figure S3). TEM images with the scale bar of 50 nm exhibit high periodicity of porosity for Beta zeolites with the pore diameter of ca. 0.4 nm (Figure S4). Figure S4d reveals different phases in bentonite (crystals and fibers) in line with XRD analysis. The length and width of the fibers were determined to be 60 and 0.9 nm, respectively, which are typical dimensions of montmorillonite [18]. In addition to a high aspect ratio, the montmorillonite fibers also showed high flexibility.

SEM images of the synthesized powder materials (Figure 5 and Figure 6) confirmed that there are not just mechanical mixtures. In composite materials, the morphological characters that cannot be clearly attributed to either of the neat materials. Red circles in the SEM images show the selected interfacial interactions of the phases for the illustration purposes. On the other hand, the neat structures of Beta zeolite and bentonite were also observed here, which were largely interconnected with a smooth bentonite bridge. Locally, small particles of Beta zeolite placed on the large bentonite particle were also observed. Beta zeolite crystallites deposited on bentonite platelets can be clearly observed in the SEM images of H-Beta-300 with the scale bar of 2 μm.

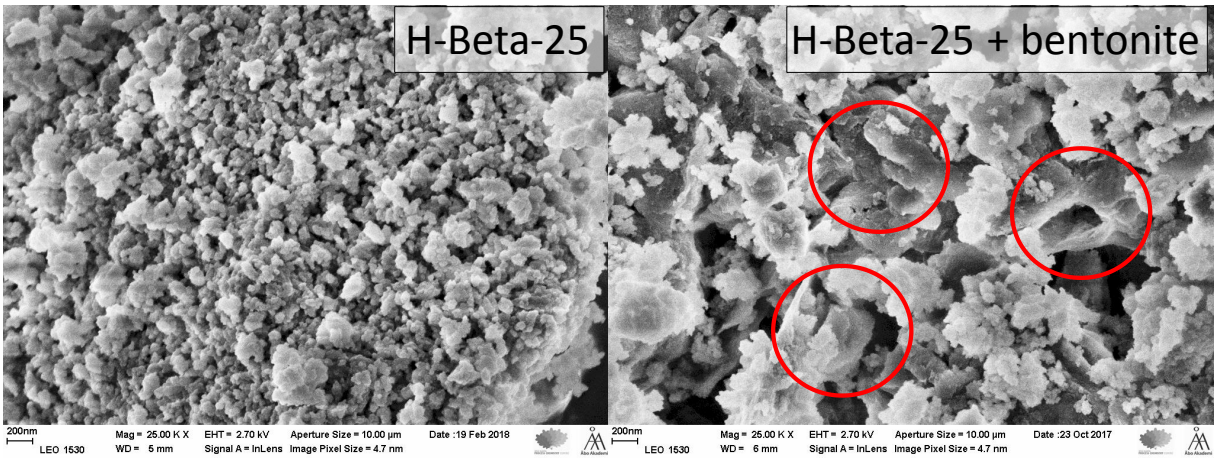

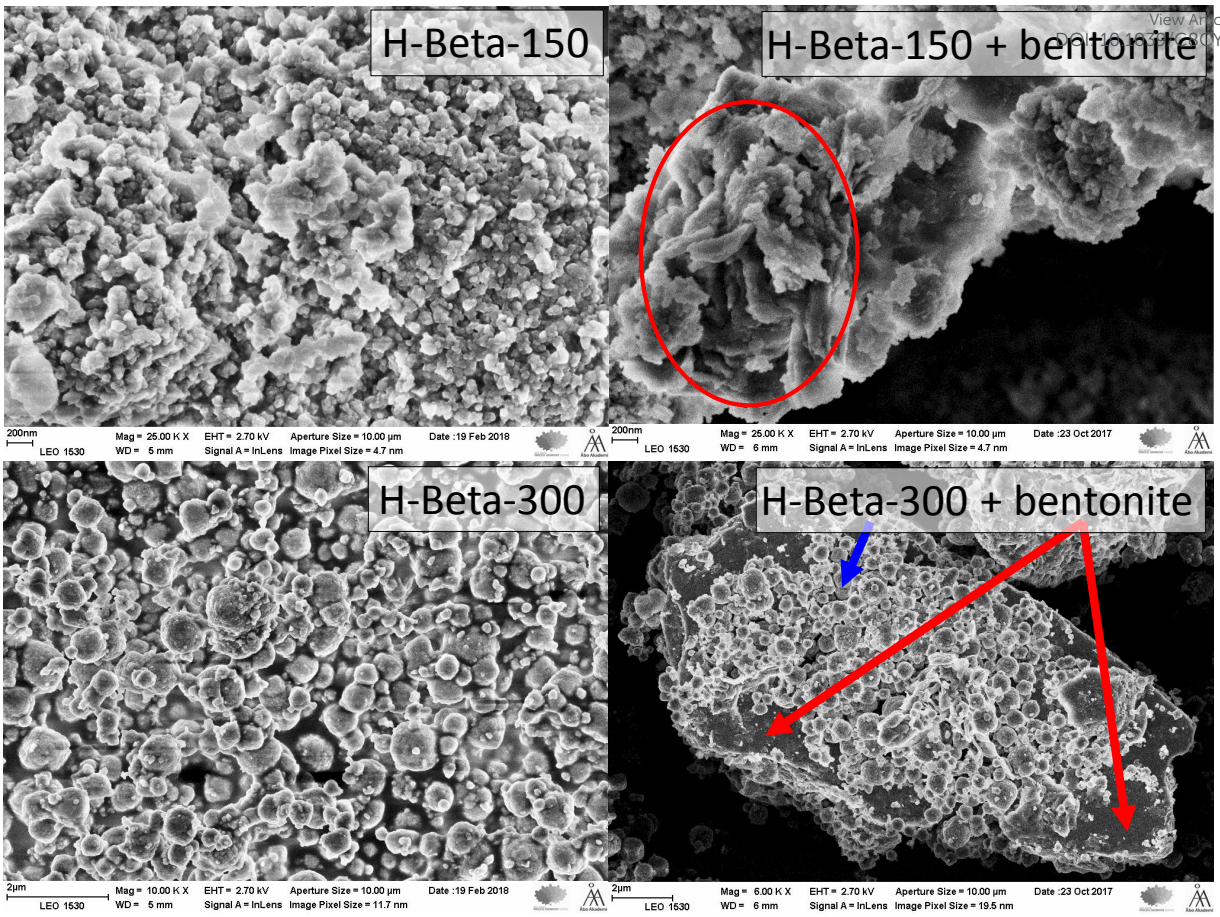

Figure 5. SEM images: Morphology of three types of pristine Beta zeolite (left) and composite materials (right). Scale bar 200, 200 nm and 2 µm for H-Beta-25, H-Beta-150 and H-Beta-300, respectively. Interfacial interactions of the phases are shown in red for illustration purposes.

TEM images of the synthesized powder mixtures show selected areas where H-Beta zeolite and the bentonite binder interact (Figure 6). The image of 80 wt.% H-Beta-300 + 20 wt.% bentonite composite again clearly confirms significant interactions of the phases in the synthesized materials. On the contrary, the image of 80 wt.% H-Beta-25 + 20 wt.% bentonite illustrates that the mixtures may also contain pure components without interactions thereby maintaining the original porosity of Beta zeolites. These pristine components without interactions with the second phase were only observed in few cases.

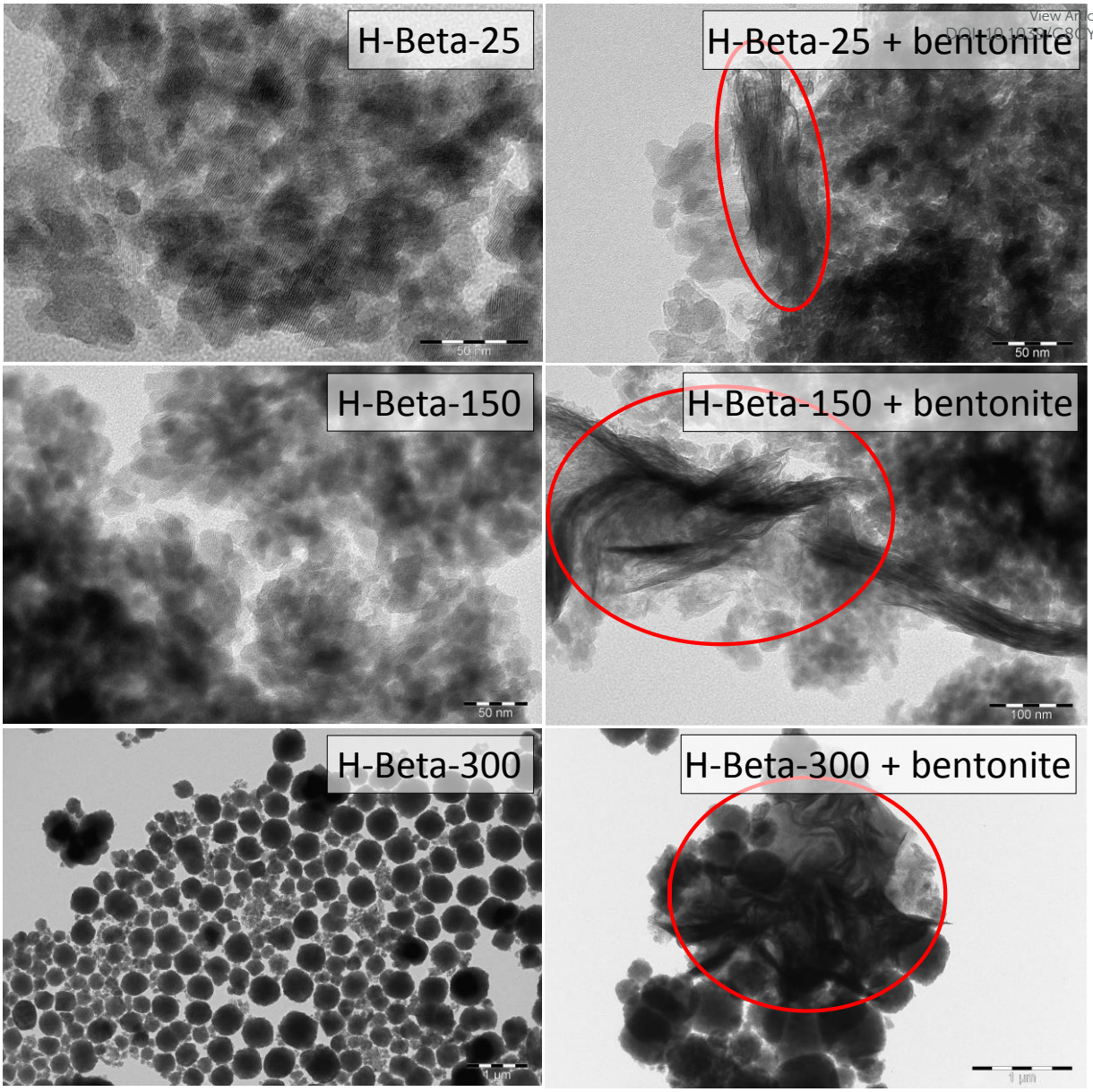

Figure 6. TEM images: Morphology of three types of pristine Beta zeolite (left) and composite materials (right). Scale bar 50, 50 – 100 nm and 1 µm for H-Beta-25, H-Beta-150 and H-Beta-300, respectively. Interfacial interactions of the phases are shown in red for illustration purposes.

3.1.4 Textural properties

Textural properties of pristine microporous materials were determined by nitrogen physisorption. The surface areas of H-Beta-25 and H-Beta-300 were 681 m^2/g and 629 m^2/g, respectively, while the surface area of H-Beta-150 was ca. 100 m^2/g lower compared to the latter one. Very similar values of specific surface areas for Beta zeolites (664 – 807 m^2/g) were presented in the work of Liu et al. [22], where the results also did not correlate with the

View Article Online
DOI: 10.1039/C8CY01951G

SiO_2/Al_2O_3 ratio. The surface area of bentonite was only 186 m^2/g. This is in line with the XRD results presented above confirming that the used bentonite consists of 80% illite in agreement with [27], reporting the specific surface areas of kaolinite, illite, and montmorillonite of ca. 15, 90 and 800 m^2/g, respectively.

Similar pore diameters of 0.4 nm were revealed by TEM for all Beta zeolites. For bentonite, it was not possible to determine the pore diameter by TEM, because only the spaces between fibers of montmorillonite were visible. The gap size between montmorillonite fibers was 0.24 nm. The highest pore volume of 0.69 cm^3/g was observed for H-Beta-25, while bentonite exhibited the lowest value.

Dependence of the specific surface areas and the micropore volume on the amount of bentonite in composites is non-linear (Figure 7). This is in line with the above presented data suggesting that the prepared composites are not simple mechanical mixtures, but exhibited clear chemical interactions. Changes in the textural properties can be attributed to the mechanical impact during ball milling.

The influence of bentonite concentration on the surface area is significant and reflects the same trend as the influence of bentonite concentration on the micropore volume. Interpretation of the bentonite concentration influence on the meso- and macropore volume is on the contrary not straightforward. The results of the composites that deviated most from the theoretical value were repeated with a relative error of less than ±10%.

For H-Beta-25 composites with 10% and 20% of bentonite concentration, the surface area was significantly lower and the meso- and macropore volume was up to 1.5 fold higher than the theoretical value. This phenomenon was also observed by Lucas et al.[29], who stated that upon shearing and agglomeration by extrusion the binder modified porosity of the zeolite providing meso- and macropores. This caused a partial blocking of the micropore mouths leading to an increase the tortuosity. It should be noted that in the current work an increase in

View Article Online
DOI: 10.1039/C8CY01951G

meso- and macropore volume was observed for the powder composites, i.e. before formation of the shaped catalysts by extrusion. It can be concluded that a partial blocking of the micropore mouths already occurs during synthesis of the composite materials also involving shearing by ball milling.

Interestingly enough such behaviour was not present for H-Beta-150 and H-Beta-300 composites. For H-Beta-300 containing materials the binder effect on the textural properties was opposite to that for Beta-25 composites, i.e. a slightly higher surface area and an extremely low meso- and macropore volume were observed compared to the theoretical values. The reason can be a significantly higher SiO_2/Al_2O_3 ratio as well as a larger particle size of the zeolite used. The same effect was observed for the USY and Beta zeolites in the work of de Lucas et al.[29], who stated that Beta zeolite crystallizes with many stacking faults, suggesting that most of their mesoporosity is associated with intra-crystalline voids. When zeolites are agglomerated the binder fills part of these mesopores and the mesoporosity loss due to the filling up of the voids is more important than mesoporosity provided by the binder. For H-Beta-150 the observed effect of the binder on the textural properties was not straightforward. For a composite with the bentonite concentration of 20%, the binder effect on the textural properties was similar to that for Beta-300 composites. For the composite with a higher bentonite concentration of 30%, the binder effect was similar to that for Beta-25 composites.

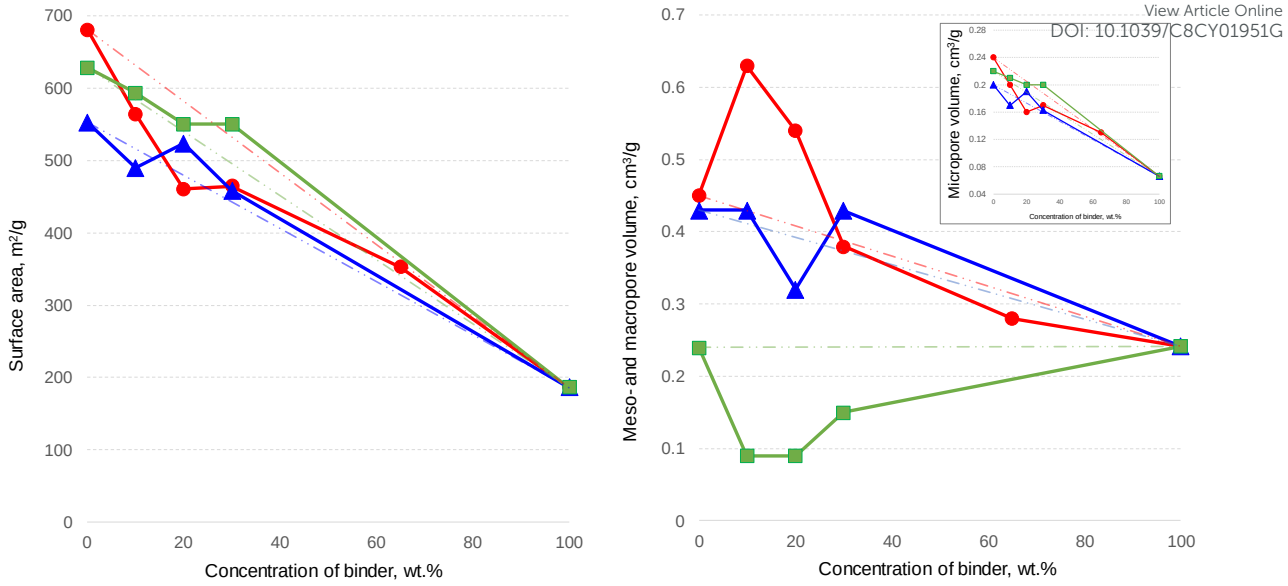

Figure 7. Influence of bentonite concentration on textural properties of three types of Beta zeolite. Legend: H-Beta-25 (red circle), H-Beta-150 (blue triangle), H-Beta-300 (green square), nominal-linear dependence (dot-dot-dash line) is shown for illustration purposes.

3.1.5 Brønsted and Lewis acid sites

In agreement with the expectations, the total acid sites of Beta zeolites are decreasing with an increase of the SiO_2/Al_2O_3 ratio. All samples contain ca. 5 fold more Brønsted acid than Lewis acid sites. The amount of weak Lewis acid sites in Beta zeolites is ca. two fold larger compared to the amount of medium and strong Lewis acid sites.

The high total acidity was observed for H-Beta-25 (349 µmol/g) and H-Beta-150 (320 µmol/g). On the contrary, an extremely low total acidity was observed for bentonite being only 23 µmol/g, although it exhibits the lowest SiO_2/Al_2O_3 ratio. This is in line with its a completely different, nonporous crystalline structure compared to Beta zeolites. The reason for a lower concentration of Brønsted acid sites in bentonite as compared to Beta zeolites is the location of Al species. Even though bentonite has the lowest SiO_2/Al_2O_3 = 5 i.e. the largest amount of bulk Al as compared to Beta zeolites. Most of Al in bentonite is located in the extra-framework resulting in small amounts of Lewis acid sites and Brønsted acid sites. Creation of Brønsted acid occurs when Al is situated in the tetra-hedra (IV) framework of the

aluminio-silicate material. Hence, Beta zeolites with Al situated in the tetrahedral (IV) framework showed the largest amount of Brønsted acid sites. The identification and location of Al in tetrahedral (IV) and extra-framework (V, VI, VIII) in the bentonite binder, H-Beta-25 and Beta-25 composite samples was performed using ^{27}Al MAS NMR and ^{29} Si NMR spectroscopy. The detailed description of NMR spectra analysis for Al speciation can be found in the supporting information Figure S5, Figure S6, Table S2 and Table S3. A very similar value of 38 µmol/g was determined for bentonite by Lucas et al. [29]. However, only weak acid sites were observed there. On the contrary, the same or higher amounts of strong and medium acid sites were reported in [29] compared to the amount of weak acid sites for bentonite in the current work.

3.1.6 Brønsted and Lewis acid sites

Reactivity and selectivity of zeolites as catalysts are determined by active sites provided by an imbalance in the charge between the silicon and aluminium ions in the framework. Each aluminium atom in the zeolite framework induces a potential active acid site. As well known acidity is typically classified as Brønsted and Lewis one [6]. The results of the composites that deviated most from the theoretical value were repeated with a relative error of less than ±9.2%.

The results revealed that acidity of the composite materials decreases non-linearly with increasing bentonite concentration. This is in line with the results presented above. Observed total acidity of all composite materials was lower than the theoretical prediction (calculated from the contribution of the raw materials: zeolite and bentonite). The largest decrease of acidity was observed for H-Beta-150 composites compared to the theoretical value. Although H-Beta-150 and H-Beta-25 zeolites are chemically, morphologically and texturally very close, H-Beta-150 composites revealed a roughly 1.4 fold higher decrease of acidity than H-Beta-25 composites compared to the theoretical values. H-Beta-300 composites showed a slight

View Article Online
DOI: 10.1039/C8CY01951G

decrease close to the theoretical value. According to the literature [17, 29-32], a decrease in the number of expected total acid sites could be attributed to a partial solid-state ion exchange between cations of the clay by protons of the zeolite during mechanical mixing. This neutralization is also responsible in part of the stability improvement, which is mainly due to the selective poisoning of active sites to prevent coke-forming reactions and trapping of the coke precursors by the binder hence decreasing coke deposition on the zeolite[32]. Such explanation of acidity decrease by ion exchange is also consistent with the results of the elemental analysis presented above.

Although the total amount of the acid sites was lower than the theoretical value, the amount of Lewis sites was significantly higher for H-Beta-25 composites with more than 30% bentonite. The same behaviour was observed for ZSM-5 with kaolin as a binder[17]. An increase in the Lewis acidity was also observed by Wu et al. 33 for ZSM-5 zeolite with alumina as a binder accompanied, however, with an increase of total acidity.

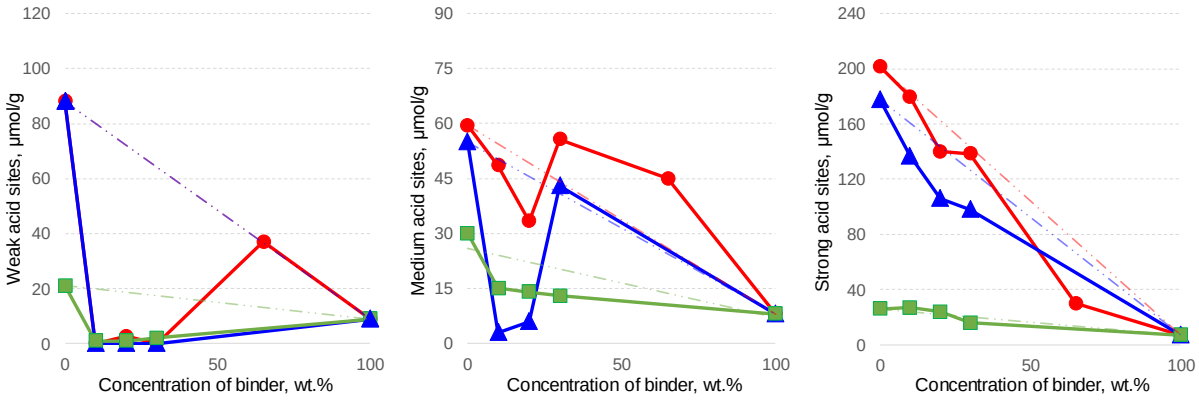

Figure 8. Influence of bentonite concentration on weak, medium and strong acidity of Beta zeolite with different SiO_2/Al_2O_3 ratios. Legend: H-Beta-25 (red circle), H-Beta-150 (blue triangle), H-Beta-300 (green square), nominal-linear dependence (dot-dot-dash line) is shown for illustration purposes.

In line with the literature[29, 33, 34], lower levels of the strong acidity than the predicted ones were observed especially for H-Beta-150 composites. On the contrary, while some studies [29,

View Article Online
DOI: 10.1039/C8CY01951G

[30] have described an increase in the weak acidity for ZSM-5, USY, mordenite and Beta composites, the opposite trend was observed in the current work. All Beta composite materials showed a significant decrease in the weak acidity (Figure 8). An exception is H-Beta-25 composite with 65% bentonite, where the weak acidity is nearly the same as the theoretical value.

3.1.7 Si and Al speciation

Figure 9 shows ^{29}Si and ^{27}Al MAS NMR spectra of the studied samples. ^{29}Si spectrum of bentonite (Figure S5) displays several lines characteristic for clay samples with a considerable amount of amorphous silica. The spectrum consists of several resonance lines. The most intense component (50% of the total intensity) at -111 ppm belongs to Q^4 sites (silicon sites in SiO_4 tetrahedra connected with four other SiO_4 units in 3D silica. The next component (22% of intensity) belongs to silicon sites in typical clay samples, which is noted as Q^3_{clay} sites in silica sheets where three nearest neighbor oxygen ions are connected to three other silicon ions in the silica layer and the fourth oxygen is connected to two Al ions in an alumina layer. The peak at -101 ppm (19%) can be assigned to silicon sites Q^3 in amorphous silica, where silicon has three SiO_4 groups and one OH group as nearest neighbors. The peak at -86 ppm (2%) is assigned to the Q^3_{clay}(1Al) sites, where one of the silicon neighbors in a silica layer is substituted by Al ions. The broad line at -84 ppm (6%) can be attributed to amorphous sites Q^2 and Q^3_{clay}(1Al) sites. A sharp peak at -107.4 ppm (0.6%) belongs to silicon in quartz. The spectrum of ^{27}Al of bentonite (Figure S6) shows the main line at 4.7 ppm from 6-coordinated aluminium sites in alumina sheets of the clay and the line at 71.7 ppm from tetrahedral aluminium sites in silica layers.

^{29}Si spectrum (Figure 9, Table S2) of B25B10 (90% H-Beta 25 +10% Bentonite) consisting of five Gaussian lines is typical for H-Beta zeolite with the lines at -115 ppm, -111 ppm from the framework T-sites and at -103 ppm from defect Q^3 sites. In addition, 44 % of

the intensity shows up as an unresolved line with a maximum at -110 ppm, which can be considered as an effect of bentonite.

^{27}Al spectrum (Table S3) of this sample is close to that of parent H-Beta zeolite with the main lines at 58 ppm and 54 ppm from tetrahedral aluminium sites and some octahedral alumina around 0 ppm. Interestingly no lines from original bentonite can be recognized. At higher bentonite concentration one can notice in ^{29}Si NMR spectra an increase of the unresolved line at -110 ppm and increase of the intensity below -100 ppm. In ^{27}Al spectra an increase of the intensity around 4 ppm from octahedral Al sites and appearance of the lines around 60-70 ppm from tetrahedral aluminium of clay can be noticed.

View Article Online
DOI: 10.1039/C8CY01951G

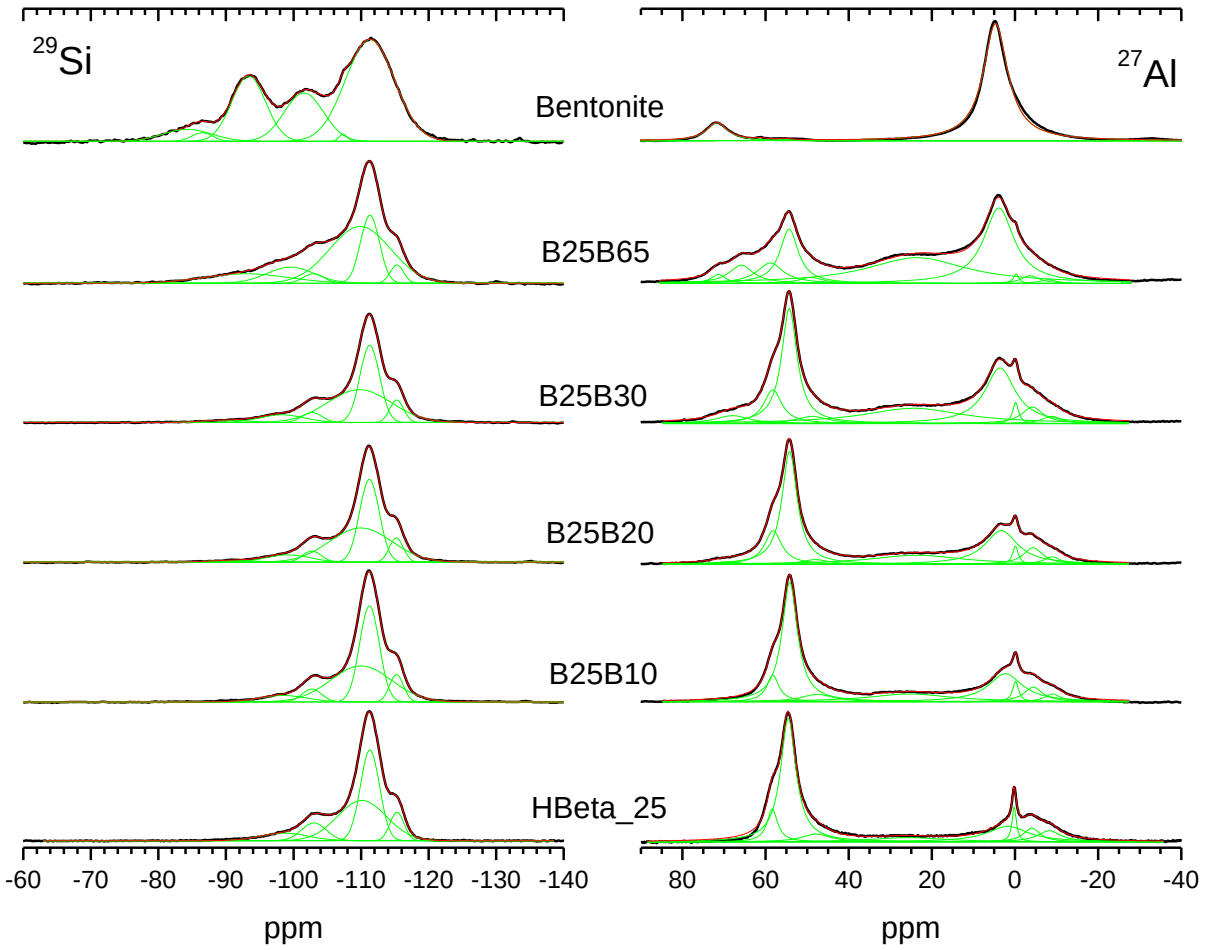

Figure 9. ^{29}Si (left) and ^{27}Al (right) MAS NMR spectra of Bentonite and Beta zeolite/Bentonite samples. Legend: B25B10: 90% H-Beta 25 +10% Bentonite; B25B20: 80% H-Beta-25 +20% Bentonite; B25B30: 70% H-Beta-25 +30% Bentonite; B25B65: 35% H-Beta-25 + 65% Bentonite.

The parameters of the lines in ^{27}Al and ^{29}Si MAS NMR spectra of all studied lines are given in Tables S2 and S3. The main trend from ^{27}Al MAS NMR seems to be that with increasing of bentonite concentration there was an increase in intensity of the line at ca. 4 ppm, which might correspond to aluminium octahedral sites in clay. The other finding is that at higher bentonite concentrations additional lines appear at 65 and 71 ppm.

Overall considering NMR spectra of bentonite, neat beta -zeolite[35] and the composites it can be concluded that these spectra reflect the non-additive character of binder-zeolite Beta-25 composites.

3.2 Effect of calcination temperature

It follows from the discussion above that a noticeable modification of the physico-chemical properties of binder containing composites of Beta zeolites in the powder form compared with the raw materials occurred already during synthesis involving mixing by just ball milling, i.e. before formation of the shaped catalysts through extrusion. For this reason, the effect of calcination temperature as a key step in the synthesis was studied by evaluating textural properties and acidity for the selected composite materials.

3.2.1 Textural properties

Influence of the calcination temperature (350 – 650 °C) on the textural properties was studied for pristine H-Beta-25 and bentonite as well as for a mixture comprising 70 wt.% H-Beta-25 and 30 wt.% bentonite (Figure 10). It has been shown, that the calcination temperature does not have a significant effect either on the composite or pristine materials in the studied temperature range. Current results are thus different from the work of Menad et al.[37] who stated that the calcination temperature plays a crucial role in the formation of LTA zeolite giving materials with varying structural features. In particular, calcination up to 700 °C increased the surface area as well as the meso- and micro-porous volume. Such behaviour different from the one observed in the current work can be attributed to stability of Beta zeolite, which is more hydrothermally stable than LTA, and to significant structural changes already occurring with the composites prepared in this study during ball milling.

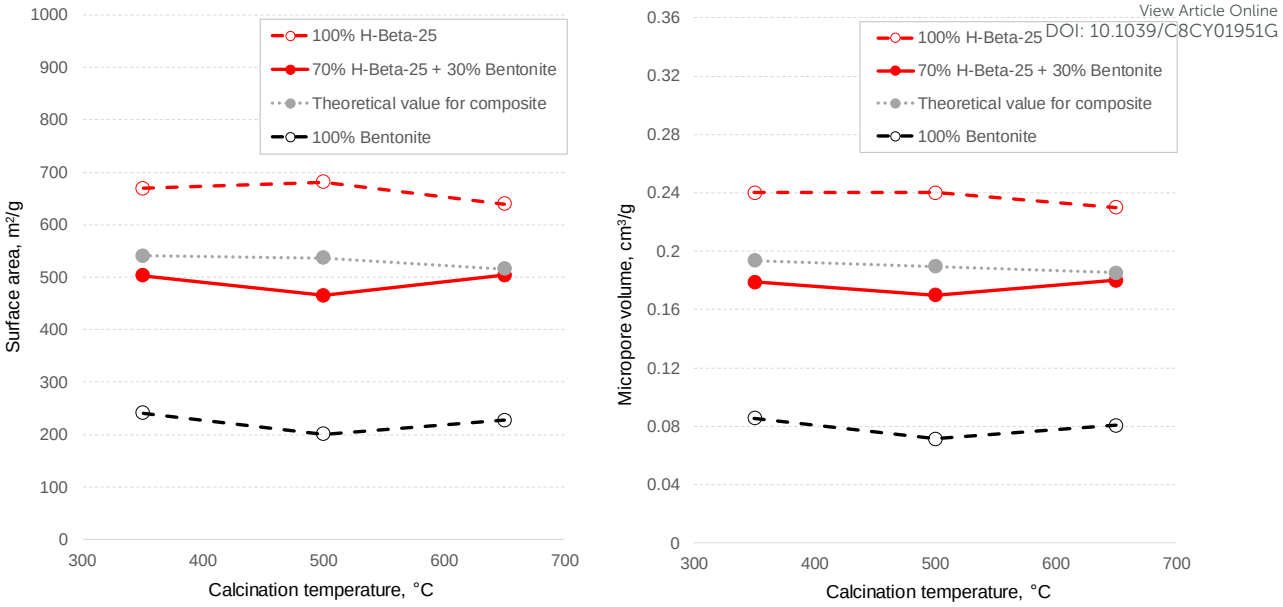

Figure 10. Dependence of a) surface area and b) microporous volume, on calcination temperature.

3.2.2 Brønsted and Lewis acid sites

While calcination temperature did not influence the surface area (Figure 10), acidity of the composite and pristine H-Beta-25 was modified by calcination (Figure 11). The total acidity and the amount of Brønsted acid sites rapidly decreased, while there were almost no changes for the amount of Lewis acid sites. As a consequence, the ratio of Lewis / Brønsted acidity was enhanced with the increase of the calcination temperature. In the work of Lu et al. [38], similar results were obtained for the HZSM-5 catalysts. In general, such decrease of acidity at high calcination temperature is attributed to dehydroxylation and dealumination [39]. A larger decrease in acidity (by 10%) was observed in the composite material. Therefore, it can be assumed that a decrease of acidity could be also attributed to chemical interactions between the phases.

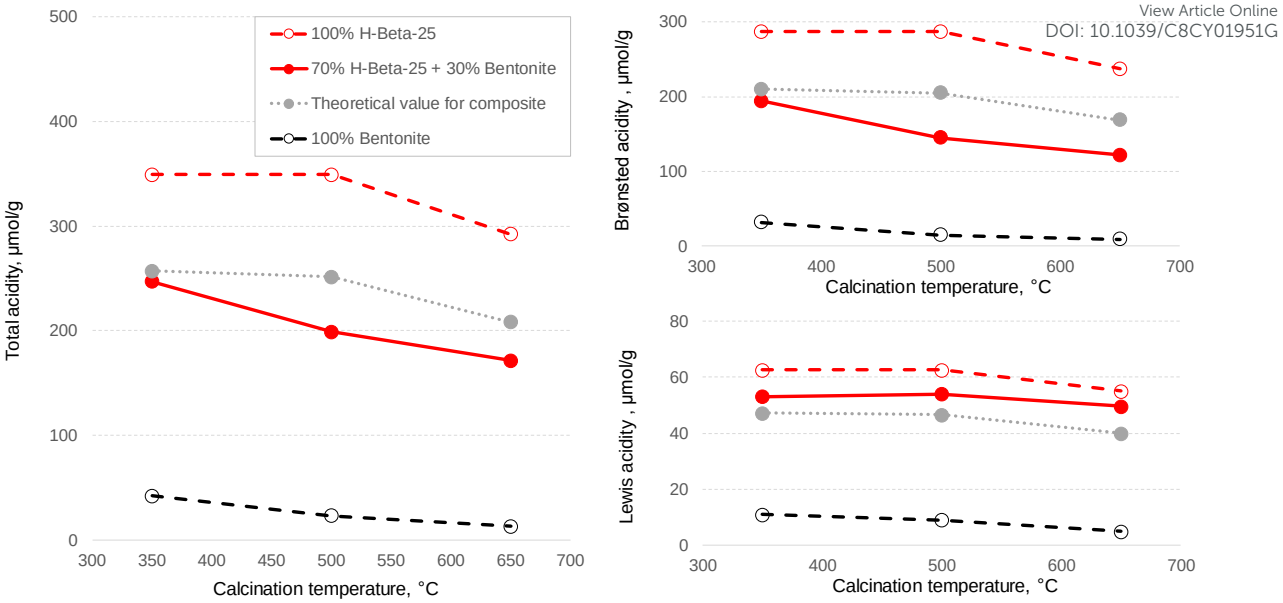

Figure 11. Acidity as a function of calcination temperature.

4 Conclusions

Composite materials for shaped catalysts were prepared from three Beta zeolites (H-Beta-25, H-Beta-150, H-Beta-300) with bentonite as an aluminosilicate clay binder (ratios 90/10, 80/20, 70/30 and 35/65). All pristine materials and the synthesized powder mixtures were characterized using several methods.

Through systematic comparison of chemical, morphological and textural properties of the individual components and powder zeolite–binder composites, a crucial binder influence on the key properties of the beta-zeolite – bentonite composites was revealed. Such influence was detected already during synthesis of powder forms by ball milling, i.e. before shaping by extrusion or tabletting. The results obtained in the current work point out on chemical interactions of bentonite with the zeolite leading to an inhomogeneous mixing of the neat materials and creation of new morphological features. As a result, properties of the composite materials are not linear combinations of components properties corresponding to the mixing ratio. With respect to different SiO_2/Al_2O_3 ratios and particle sizes of Beta zeolites, significant differences were observed in morphology and porosity of the composite materials.

View Article Online
DOI: 10.1039/C8CY01951G

Significantly lower meso- and macro pore volumes than expected for simple mechanical mixtures were observed for the composites of beta-zeolite with a high SiO_2/Al_2O_3 ratio (102 mol/mol) and a large particle size (300 nm). In other cases, the effect of the interfacial zeolite-binder interactions on the composite properties was significantly larger than the effect of the Beta zeolite per ser. For H-Beta-25 composite calcination temperature was influencing acidity, while textural properties were almost unchanged.

Understanding of the complex morphological and chemical interactions within zeolite−binder composites and procedures for their effective fine-tuning will ultimately accelerate development of shaped catalysts with superior catalytic performance.

5 Acknowledgments

The authors are grateful to Academy of Finland for funding through the project: Synthesis of spatially controlled catalysts with superior performance. The work was also supported by the Estonian Research Agency grant IUT23-7 and the European Regional Development Fund project TK134.

View Article Online
DOI: 10.1039/C8CY01951G

References

1. G. T. Whiting, F. Meirer, M. M. Mertens, A. J. Bons, B. M. Weiss, P. A. Stevens, E. de Smit and B. M. Weckhuysen, *ChemCatChem*, 2015, **7**, 1312-1321.
2. J. Zecevic, G. Vanbutsele, K. P. de Jong and J. A. Martens, *Nature*, 2015, **528**, 245-254.
3. F. Dorado, R. Romero and P. Canizares, *Applied Catalysis A: General*, 2002, **236**, 235-243.
4. R. V. Jasra, B. Tyagi, Y. M. Badheka, V. N. Choudary and T. S. G. Bhat, *Industrial & Engineering Chemistry Research*, 2003, **42**, 3263-3272.
5. S. Suresh and S. Sundaramoorthy, *Green Chemical Engineering: An Introduction to Catalysis, Kinetics, and Chemical Processes*, CRC Press, 2014.
6. V. Kaucic, *Croatica Chemica Acta*, 1994, **67**, 241-261.
7. F. Dorado, R. Romero and P. Canizares, *Industrial & Engineering Chemistry Research*, 2001, **40**, 3428-3434.
8. H. Liu, Y. M. Zhou, Y. W. Zhang, L. Y. Bai and M. H. Tang, *Industrial & Engineering Chemistry Research*, 2008, **47**, 8142-8147.
9. J. S. J. Hargreaves and A. L. Munnoch, *Catalysis Science & Technology*, 2013, **3**, 1165-1171.
10. N. Y. Chen, M. C. Liu, S. C. Yang, H. S. Sheu and J. R. Chang, *Industrial & Engineering Chemistry Research*, 2015, **54**, 8456-8468.
11. W. J. Roth and J. Cejka, *Catalysis Science & Technology*, 2011, **1**, 43-53.
12. S. Mitchell, N. L. Michels and J. Perez-Ramirez, *Chemical Society Reviews*, 2013, **42**, 6094-6112.
13. S. P. Verkleij, G. T. Whiting, S. P. Esclapez, M. M. Mertens, A. J. Bons, M. Burgers and B. M. Weckhuysen, *Catalysis Science & Technology*, 2018, **8**, 2175-2185.
14. G. T. Whiting, A. D. Chowdhury, R. Oord, P. Paalanen and B. M. Weckhuysen, *Faraday Discussions*, 2016, **188**, 369-386.
15. G. T. Whiting, F. Meirer, M. M. Mertens, A. J. Bons, B. M. Weiss, P. A. Stevens, E. de Smit and B. M. Weckhuysen, *Chemcatchem*, 2015, **7**, 1312-1321.
16. A. J. Martin, S. Mitchell, K. Kunze, K. C. Westonc and J. Perez-Ramirez, *Materials Horizons*, 2017, **4**, 857-861.
17. N. L. Michels, S. Mitchell and J. Perez-Ramirez, *ACS Catalysis*, 2014, **4**, 2409-2417.
18. R. D. Holtz, W. D. Kovacs and T. C. Sheahan, *An Introduction to Geotechnical Engineering*, Prentice-Hall, 1981.

19. M. A. Uguina, J. L. Sotelo and D. P. Serrano, *Applied Catalysis A: General*, 1991, **76**, 183-198.

20. G. Lagaly and S. Ziesmer, *Advances in Colloid and Interface Science*, 2003, **100**, 105-128.

21. C. H. Zhou, *Applied Clay Science*, 2011, **53**, 87-96.

22. D. Gournis, L. Jankovic, E. Maccallini, D. Benne, P. Rudolf, J. F. Colomer, C. Sooambar, V. Georgakilas, M. Prato, M. Fanti, F. Zerbetto, G. H. Sarova and D. M. Guldi, *Journal of the American Chemical Society*, 2006, **128**, 6154-6163.

23. V. C. Kelessidis and R. Maglione, *Colloids and Surfaces A: Physicochemical and Engineering Aspects*, 2008, **318**, 217-226.

24. J. K. Mitchell and K. Soga, *Fundamentals of Solid Behavior*, John Wiley & Sons, Unite States of America, 2005.

25. G. Horvath and K. Kawazoe, *Journal of Chemical Engineering of Japan*, 1983, **16**, 470-475.

26. C. A. Emeis, *Journal of Catalysis*, 1993, **141**, 347-354.

27. B. M. Das, *Advanced Soil Mechanics*, CRC Press, 2013.

28. X. Liu, P. Mäki-Arvela, A. Aho, Z. Vajglová, V. M. Gun´ko, I. Heinmaa, N. Kumar, K. Eränen, T. Salmi and D. Y. Murzin, *Molecules*, 2018, **23**, 946.

29. A. de Lucas, P. Sanchez, A. Funez, M. J. Ramos and J. L. Valverde, *Industrial & Engineering Chemistry Research*, 2006, **45**, 8852-8859.

30. M. D. Romero, J. A. Calles, A. Rodriguez and A. deLucas, *Microporous Materials*, 1997, **9**, 221-228.

31. V. R. Choudhary, P. Devadas, A. K. Kinage and M. Guisnet, *Applied Catalysis A: General*, 1997, **162**, 223-233.

32. J. M. Fougerit, N. S. Gnep, M. Guisnet, P. Amigues, J. L. Duplan and F. Hugues, *Studies in Surface Science and Catalysis*, 1994, **84**, 1723-1730.

33. X. Wu, A. Alkhawaldeh and R. G. Anthony, *Studies in Surface Science and Catalysis*, 2002, **143**, 217-225.

34. A. de Lucas, J. L. Valverde, P. Sanchez, F. Dorado and M. J. Ramos, *Industrial & Engineering Chemistry Research*, 2004, **43**, 8217-8225.

35. K. Yu, N. Kumar, A.Aho, J. Roine, I. Heinmaa, D.Yu. Murzin and A. Ivaska, *Journal of Catalysis*, 2016, **335**, 117-124

36. A. Aho, N. Kumar, K. Eränen, M. Hupa, T. Salmi and D. Yu. Murzin, *Studies in Surface Science and Catalysis*, 2008, **174B**, 1069-1074.

37. K. Menad, A. Feddag and K. Rubenis, *Rasayan Journal of Chemistry*, 2016, **9**, 788-797.

38. J. Lu, Z. Zhao, C. Xu, A. Duan and P. Zhang, *Journal of Natural Gas,* 2005, **14**, 213-220.

39. A. Auroux, *Acidity and Basicity: Determination by Adsorption Microcalorimetry*, Springer, Berlin, Heidelberg, 2006.